JOURNAL OF PROPULSION AND POWER
Vol. 30, No. 2, March–April 2014

Effect of External Cathode Azimuthal Position on Hall-Effect Thruster Plume and Diagnostics

Kunning G. Xu*
University of Alabama, Huntsville, Alabama 35899
and
Mitchell L. R. Walker†
Georgia Institute of Technology, Atlanta, Georgia 30332

DOI: 10.2514/1.B34980

The T-220HT Hall-effect thruster was tested with the external cathode at different azimuthal locations to determine the effect of an external cathode on the far-field plume. The cathode is mounted in two configurations: 1) on top of the thruster, perpendicular to the plane of plume measurements, and 2) in the plane of plume measurements. The thruster was tested at discharge voltages of 150–300 V at a constant discharge current of 9 A on krypton propellant. The vacuum facility operating pressure was below 9.2×10^{-6} torr · Kr for all operating conditions. Noticeable changes in the plume ion current density were measured that indicate plume asymmetry. With the cathode in the plane of the probes, the ion current density peak increases by up to 43% and the divergence angle decreases by up to 2.6 deg. However, there is less than a 5 V shift in the ion energy distribution, and the distribution shape remains constant. The results indicate that an external cathode alters the plume symmetry and creates a region of increased ion flux. An analysis of the cathode generated species densities indicates that the increase in ion current density is caused by nonuniform ingestion of cathode neutrals and nonuniform electron density near the cathode. This phenomenon can affect thruster plume measurements as well as the orientation of thrusters for satellite integration.

I. Introduction

The operation and testing of Hall-effect thrusters (HETs) are influenced by many variables, such as propellant mass flow rate, vacuum chamber operating pressure, chamber size, probe size and distance, and cathode location. This paper is focused on the last variable, specifically the effect of azimuthal cathode location on the HET plume. The cathode is an integral part of the HET. It acts as the negative electrode of the thruster discharge electrical circuit. The cathode supplies electrons to the Hall current for ionization of the propellant, as well as to the plume for neutralization of exhaust ions. The location of the cathode has a large effect on the performance of the thruster. HET cathodes are mounted either internally, at the center of the thruster body, or externally, outside of the thruster body. Internal cathodes universally give better performance than external cathodes, but are not always an option. Small thrusters such as the BHT-200 and cylindrical thrusters [1] cannot accommodate an internal cathode, and existing thrusters such as the T-220HT used in this work were designed for external cathode use and are unlikely to be redesigned.

Figure 1 shows a diagram of the various cathode mounting positions for an HET along with a typical plume measurement plane. Previous research into cathode effects has examined cathode mass flow rate [2], center versus external mounting [2,3], and distance from the thruster [3,4]. The asymmetric effect of an external cathode has also been examined in recent years. Parra and Ahedo [5] numerically showed the existence of an asymmetric potential distribution inside the discharge chamber due to an external cathode. More recently, Bourgeois et al. [6] used laser induced fluorescence of Xe ions to measure the azimuthal ion velocity inside a HET channel. The results showed differences in the azimuthal velocities depending on the location within the channel. The velocity asymmetry was attributed to the negative potential of cathode attracting ions, thus increasing azimuthal ion velocity near the cathode. Likewise, Ellison et al. [7] took high-speed images of a HET ignition and showed the presence of a start-up asymmetry due to the cathode position. However, shortly after ignition, ~50 μs, the asymmetry disappears. This work examines the azimuthal nonuniformity an external cathode produces in the Hall thruster plume by sampling both in the plane of the external cathode and 90 deg out of the cathode plane.

As noted by other researchers, the position of an external cathode relative to the thruster can affect performance. HETs are axisymmetric devices, thus their plume parameters are also assumed axisymmetric; however, as the cathode provides the primary source of electrons, its location may affect the plume distribution, which can introduce asymmetric behavior. This would have implications for future HET vacuum testing as well as satellite integration. Possible effects include plume impingement due to increased divergence angles, shift of the center of thrust, and errors in reported plume angles and ion currents. This work examines the plume profile for a modified T-220HT HET with the cathode in the out-of-plane and in-plane positions relative to the plume measurement plane as shown in Fig. 1. Section II discusses the experimental setup. Section III presents the results of the plume measurements. Section IV presents an analysis of cathode particle densities and provides an explanation for the observed results.

II. Experimental Setup

A. Hall Thruster

All experiments are performed on a modified Pratt and Whitney Rocketdyne T-220HT HET. Extensive testing has mapped the performance of the base thruster over a power range of 2–22 kW at discharge voltages of 200–600 V [8]. The T-220HT has a mean channel diameter of 188 mm and a nominal power rating of 10 kW. The discharge channel of the thruster is made of M26 grade boron nitride. A more detailed description of the T-220HT and its characteristics can be found in [4]. The T-220HT HET discharge supply is a 45 kW Magna-Power TSA800-54 power supply, and all other thruster components are powered with TDK-Lambda 1 or 3.3 kW Genesys power supplies. All electrical connections enter the chamber through separate feedthroughs. The thruster discharge

Received 6 March 2013; revision received 30 July 2013; accepted for publication 11 September 2013; published online 10 February 2014.

*Assistant Professor, Mechanical and Aerospace Engineering, S234 Technology Hall. Member AIAA.

†Associate Professor, Aerospace Engineering, High-Power Electric Propulsion Laboratory, 270 Ferst Drive NW. Associate Fellow AIAA.

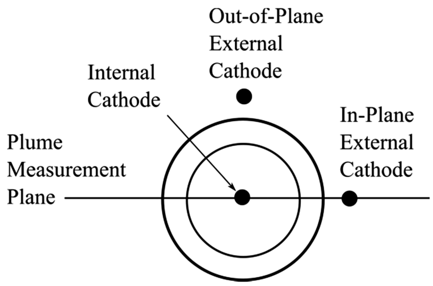

Fig. 1 A frontal diagram of an HET showing three typical cathode locations used in HETs along with the orientation of planar plume measurements. Out-of-plane and in-plane cathodes will be used to designate the two configurations tested in this work.

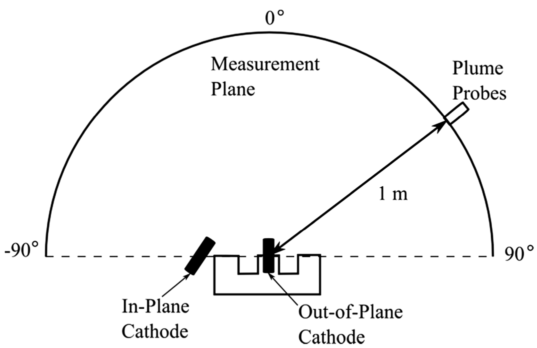

Fig. 2 Top view of cathode positions relative to the plume measurement plane. Although not apparent from this angle, the cathode is declined 45 deg toward the thruster centerline.

supply is connected to a resistor–capacitor filter consisting of a 1.3 Ω resistance and 95 μF capacitor. The filter acts as a low-pass filter preventing oscillations in the discharge current over 1.4 kHz from reaching the discharge supply. High-purity (99.9995%) krypton propellant is supplied with MKS 1179A mass flow controllers to the cathode and anode with an uncertainty of ± 0.03 and ± 0.2 mg/s, respectively. The thruster discharge current is held constant at 9 ± 0.05 A. The anode flow rate varied from 7.08 to 8.86 mg/s over the conditions tested.

A commercial cathode, the Electric Propulsion Laboratory (EPL) 375 series, is used in this work [9]. It is mounted first in the out-of-plane position for testing, then moved to the in-plane position and tested. The thruster and diagnostics are unchanged between two cathode positions, thus allowing for measurement of the same plume and thruster locations. In both cases, the cathode is aligned approximately 45 deg with the thruster centerline as to be aligned with the local magnetic field. The cathode orifice is located approximately 1.5 cm downstream from the thruster exit plane. The cathode flow rate is set to a constant 1 mg/s for all cases investigated. For the results reported here, the thruster was tested with the cathode located in two positions as shown in Fig. 2, perpendicular to the measurement plane (out of plane) and in the plane of the probe measurement sweep (in plane).

B. Faraday Probe

The Faraday probe is a simple plasma diagnostic used to measure ion current density in the HET plume [10–14]. The probe is based on the Jet Propulsion Laboratory nude Faraday probe design [11]. It consists of a 2.31-cm-diam tungsten-coated stainless steel collection electrode with a stainless steel guard ring surrounding it. A gap of 0.12 cm exists between the electrode and guard ring. A Lambda GENH 60-12.5 power supply biases the collector and guard ring to 20 V below ground. Biasing the collector and guard ring to the same potential reduces edge effects by creating a uniform sheath potential around the collector. Twenty volts was chosen based on prior experience indicating that ion saturation is reached without substantial sheath growth for this type of Faraday probe [11,12]. Voltage measurements across a 1.417 kΩ, 0.5 W resistor placed in series with the collector line are read by an Agilent 34980A data acquisition unit.

The collector surface is placed 1 m downstream of the thruster exit plane as shown in Fig. 2. The center of rotation of the probe arm is located over the thruster exit plane along the thruster centerline as shown in Fig. 2. Sweeps are taken from −90 to +90 deg from thruster centerline in 1 deg increments. Measurements are taken at a 80 Hz sample rate for 1 s at each position and averaged to produce the recorded current density at that location. The uncertainty in Faraday probe measurements caused by systematic (mechanical and electronic sources) and charge-exchange collisions is estimated at $\pm 10\%$ based on corrections developed by Brown and Gallimore [14,15]. The total uncertainly for the ion beam current calculation is thus taken at 10%. The uncertainly in the plume divergence angle is obtained through analysis of variance and is a maximum of 10% as well.

C. Retarding Potential Analyzer

A retarding potential analyzer (RPA) measures ion energy per charge with a series of biased grids to selectively filter ions [16,17]. The RPA cannot discriminate between singly and multiply charged ions. The RPA acts as a high-pass filter that only allows ions with energy higher than the ion repulsion grid to pass through to the collector. By increasing the voltage on the ion retarding grid, ions with equal or less energy are repelled and the collected current drops. The negative derivative of the resulting current-voltage data, $-\mathrm{d}I/\mathrm{d}V$, is proportional to the ion energy distribution function [16].

The RPA used in this work consists of four grids. In order from plasma to collector, they are the floating, electron repulsion, ion repulsion, and electron suppression grids [18]. The floating grid floats to the plasma potential to reduce perturbations caused by the probe presence. The electron repulsion grid is negatively biased with respect to ground to repel plasma electrons, and the ion repulsion grid is positively biased with respect to ground to retard ions. The electron suppression grid is biased negative with respect to ground to repel any secondary electrons emitted from the collector due to ion collisions. The electron repulsion and suppression grids are both held at −30 V by a pair of GENH 60-12.5 power supplies. The ion repulsion grid is powered by a Keithley 2410 sourcemeter. The collector current is measured with a Keithley 6487 picoammeter. Both the sourcemeter and picoammeter are controlled with LabVIEW. The ion repulsion grid is scanned in 1 V increments from 0 to 400 V for all operating conditions. Three measurements are taken and averaged at each grid voltage to provide the recorded value. The ion energy is obtain from the derivative of the measure ion current with respect to the repulsion grid voltage, $-\mathrm{d}I/\mathrm{d}V$. The uncertainty in the most probable ion potential is estimated as 50% of the half-width at half-maximum value of the potential peak [19].

D. Vacuum Facility

All experiments were performed in Vacuum Test Facility 2 (VTF-2) at Georgia Institute of Technology. VTF-2 is a stainless steel chamber 9.2 m long and 4.9 m in diameter. It is pumped to rough vacuum with one 3800 CFM blower and one 495 CFM rotary vane pump. Ten liquid nitrogen cooled CVI TMI reentrant cryopumps with a combined pumping speed of 350,000 l/s on xenon bring the chamber to a base pressure of 5×10^{-9} torr. The Stirling Cryogenics SPC-8 RL Special Closed-Looped Nitrogen Liquefaction System supplies liquid nitrogen to the cryopump shrouds. Two ionization gauges, Varian 571 and UHV-24, are mounted on either side of the chamber in line with the thruster. The pressure is corrected for krypton by Eq. (1):

$$\frac{P_{\mathrm{gauge}} - P_{\mathrm{base}}}{1.96} + P_{\mathrm{base}} \tag{1}$$

where P_{base} is the base pressure without a propellant flow, P_{gauge} is the ionization gauge reading during operation, and 1.96 is the correction factor for krypton [20,21]. The corrected pressures from the two gauges were averaged to obtain the operating pressure.

III. Results

To characterize the plume behavior for the two cathode positions, the thruster was tested over the range of 150–300 V in 50 V increments, all at 9 A discharge current. The test conditions for the data presented here are available in Table A1. The cathode flow rate was held constant at 1 mg/s of krypton, and 0.15 A at <1 V was maintained on the cathode keeper for all tests. Current was maintained on the keeper to reduce downtime in the event of an unexpected thruster shutdown. The thruster magnetic field was also held constant through all tests. Faraday and RPA data were taken for both the out-of-plane and in-plane cathode locations in two separate tests. The vacuum chamber was opened in between tests in order to relocate the cathode. The maximum operating pressure was 9.2×10^{-6} torr · Kr for all data.

A. Plume Current Density

The plume current density is obtained from the Faraday probe data by dividing the measured ion current by the probe collector area. The ion current density is then integrated over a hemisphere to obtain the total ion beam current. The method developed by Brown and Gallimore to account for probe gap current and dual point source is used here [14,15]. Figures 3–6 show the ion current density from −90 to +90 deg for both cathode locations. The out-of-plane position will be taken as the baseline for comparisons. For the in-plane position, the cathode is located at the left side of Figs. 3–6 at −90 deg. The results for the in-plane configuration showed two major differences in the ion flux compared with the out-of-plane configuration: increased left-hand peak and shift of the ion flux at large angles.

The first difference, the increased left peak, can be seen at all voltages. The two peaks in the data correspond to the two sides of the annular channel the probe sees in the planar sweep. For large thrusters such as the T-220HT, the plume has a focal length longer than 1 m, thus the double peak is observed [8]. The in-plane cathode increases the value of the left peak by 37, 43, 34, and 18%, compared with the out-of-plane cathode for 300, 250, 275, and 150 V discharges, respectively.

The second difference, the change in the ion current density in the wings, exists at all voltages. The right side of the plot at +90 deg shows an increase in the ion current density, whereas the left side shows a decrease. The differences in current density are observed at >|30 deg| from the thruster centerline. This does not appear to be simply a shifted profile due to probe misalignment. The in-plane configuration noticeably results in a decreased ion current density along the left-hand side (at negative angles). The uncertainty in the current density measurements is estimated at ±10%. Error bars are shown in the plots at two locations, one in the wing and one at the peak to preserve readability. The change in measured current density is larger than the error. The difference between the two profiles at each operating condition appears to be identical and systematic, thus it cannot be caused by random measurement error.

Table 1 shows the operating conditions and the calculated beam current from the Faraday probe. Lower discharge voltages required an increase in anode mass flow rate to maintain ~9 A total discharge current (the cathode flow rate was constant at 1 mg/s). The ion beam current decreases at lower discharge voltages due to lower ionization

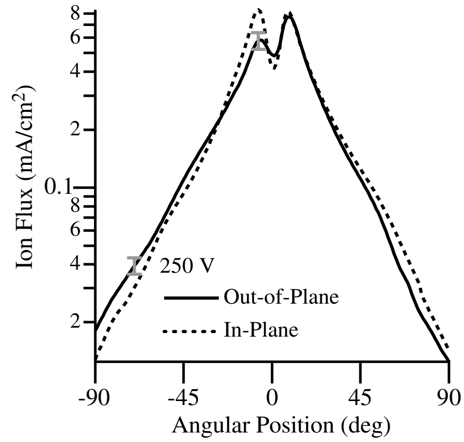

Fig. 4 Ion flux for out-of-plane and in-plane cathodes at 250 V, 9 A. Left peak maximum current density increases by 43%. Error bars for the ±10% are only shown at −70 and −7 deg for readability.

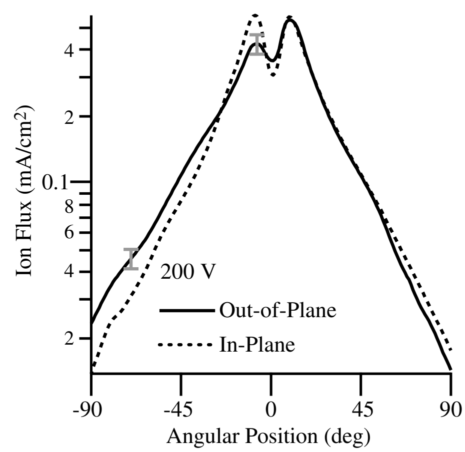

Fig. 5 Ion flux for out-of-plane and in-plane cathodes at 200 V, 9 A. Left peak maximum current density increases by 34%. Error bars for the ±10% are only shown at −70 and −7 deg for readability.

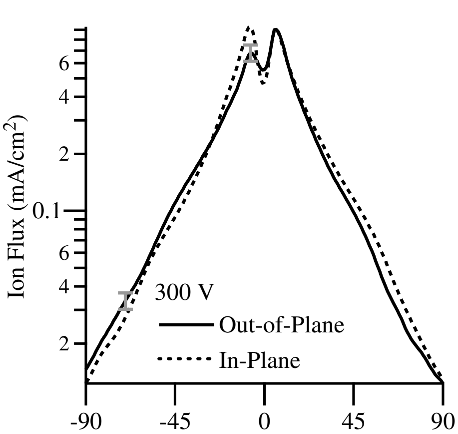

Fig. 3 Ion flux for out-of-plane and in-plane cathodes at 300 V, 9 A. Left peak maximum current density increases by 37%. Error bars for the ±10% are only shown at −70 and −7 deg for readability.

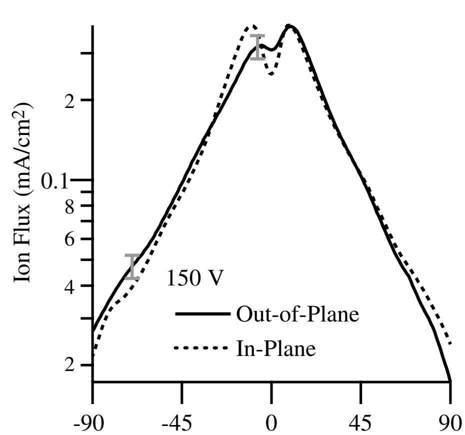

Fig. 6 Ion flux for out-of-plane and in-plane cathodes at 150 V, 9 A. Left peak maximum current density increases by 18%. Error bars for the ±10% are only shown at −70 and −7 deg for readability.

Table 1 Operating conditions and beam current for configurations tested, where the total mass flow rate includes a constant 1 mg/s of cathode flow

Cathode location	Discharge voltage V_d, V	Discharge current I_d, A	Total mass flow $\dot{m}$, mg/s	Beam current I_b, A	$I_b/\dot{m}$
Out of plane	300	8.98	8.08	6.33	0.78
	250	9.05	9.1	6.64	0.73
	200	8.95	9.26	6.19	0.67
	150	8.95	9.86	5.65	0.57
In plane	300	9.03	8.29	6.76	0.82
	250	9.02	8.5	6.98	0.82
	200	9.01	8.64	6.21	0.72
	150	9.02	8.85	5.68	0.64

rates at low voltages. The in-plane configuration produces a larger ion beam current for less mass flow compared with the out-of-plane configuration, except at 300 V, though the beam current per unit of propellant mass is higher.

Figure 7 shows the calculated plume divergence half-angle using the method by Brown and Gallimore [14,15]. Measurements made with the in-plane cathode show a decreased plume angle compared with the out-of-plane cathode. This can be attributed to a higher-density left wing of the ion current density profile in the out-of-plane cathode configuration. There is a large degree of uncertainty in the plume divergence angle (±10%), which is typical of such measurements; however, the errors are systematic rather than random.

B. Ion Energy

The ion energy distribution was measured with the RPA along the thruster centerline for the out-of-plane and in-plane cathode configurations for the 150 and 300 V cases. Figures 8 and 9 show the RPA data along the thruster centerline. Both the raw RPA current (left axis) and the calculated ion energy distribution (right axis) are shown. The most probable energies for the 300 V discharge are identical within the uncertainty (out-of-plane cathode = 259.6 V, in-plane cathode = 257.7 V). The same is seen at lower voltages. The RPA data indicate that cathode location has no effect on the thruster ion energy. The ions produced by the cathode are typically low energies compared with the thruster ions. Friedly and Wilbur [22] and Kameyama and Wilbur [23] showed that hollow cathodes can produce ions with energy greater than the electrode potential, however the energies were less than 60 V even at high cathode currents of 20–30 A. Compared with the thruster ions at 100 V+, the cathode ions do not contribute significantly to the energy distribution at the thruster centerline.

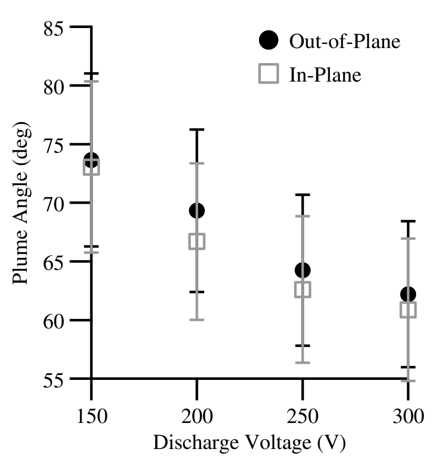

Fig. 7 Plume divergence angle for the out-of-plane and in-plane cathodes.

A second set of RPA measurements was taken at −60 deg, on the left-hand side of the thruster (refer to Fig. 2). The calculated ion energy distributions are shown in Figs. 10 and 11. The resulting energy distribution is very noisy, which is to be expected because at large angles there are fewer discharge ions and increased presence of charge-exchange ions, resulting in a large spread of possible energies. In the 300 V case, there is no noticeable change between the two cathode locations. However, at 150 V, the in-plane cathode causes an increase in the most probable ion energy by 5 V. This is outside the

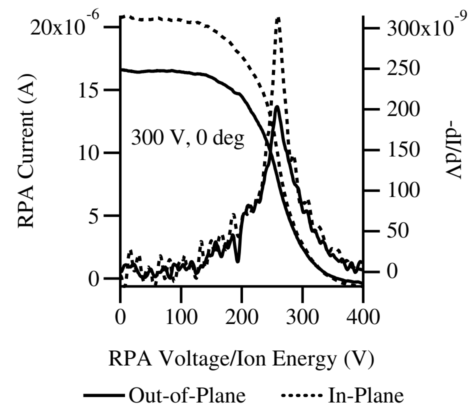

Fig. 8 RPA data for 300 V discharge along the thruster centerline. Both out-of-plane and in-plane cathodes have similar ion energy distributions, with the current level differing due to a lower minimum for the in-plane location. Most probable ion energy: out-of-plane cathode = 259.6 ± 4 V, in-plane cathode = 257.7 ± 2.4 V.

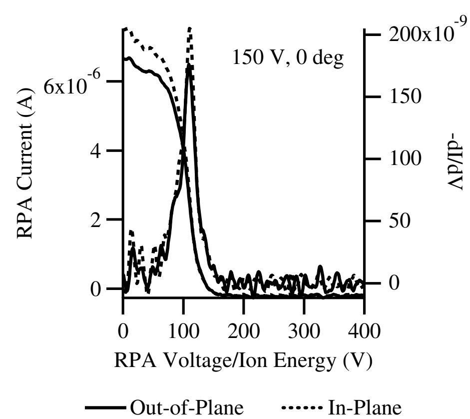

Fig. 9 RPA data for 150 V discharge along the thruster centerline. Most probable ion energy: out-of-plane cathode = 107.1 ± 7 V, in-plane cathode = 106.9 ± 7.2 V.

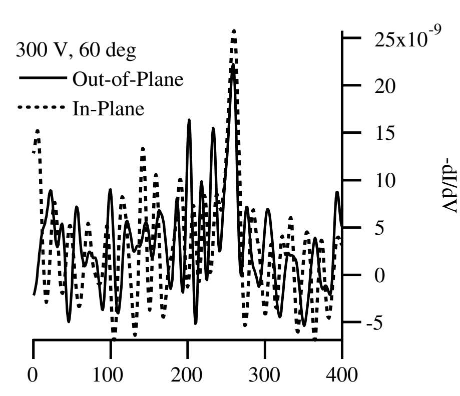

Fig. 10 RPA data for 300 V discharge at 60 deg. Most probable ion energy: out-of-plane cathode = 257.9 ± 2.2 V, in-plane cathode = 260 ± 2.4 V.

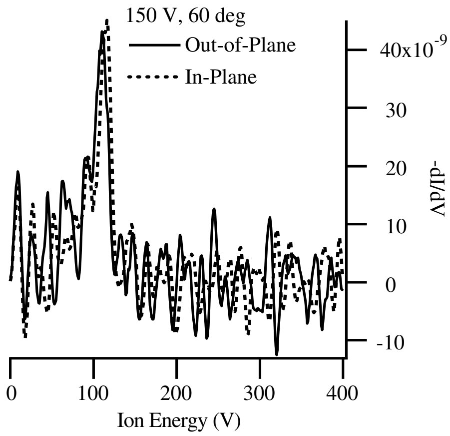

Fig. 11 RPA data for 150 V discharge at 60 deg. Most probable ion energy: out-of-plane cathode $= 110.2 \pm 2.2$ V, in-plane cathode $= 115.2 \pm 2.3$ V.

uncertainty of the measurement. This increase can be attributed to an increase in voltage utilization due to an increase in the ionization near the cathode location; i.e., near the cathode, ions are generated further upstream. However, the majority of ion energy measurements are taken along thruster centerline where cathode location appears to have no effect.

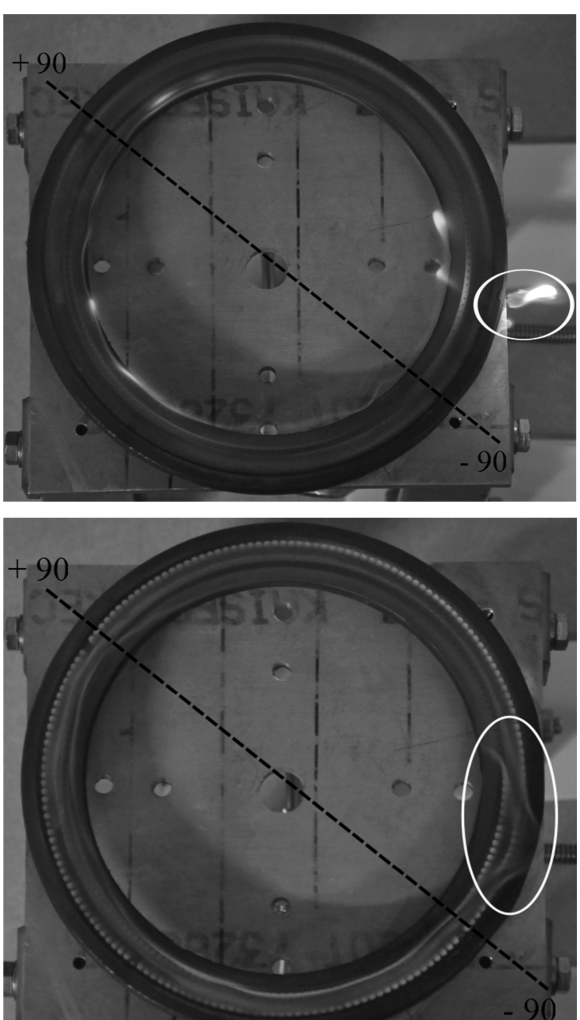

Fig. 12 Flame visualization of the anode propellant uniformity. A large leak is observed near −90 deg at fuel rich conditions (top), whereas at stoichiometric conditions the leak results in a nonuniform propellant distribution (bottom).

IV. Discussion

The results show a distinct change in plume ion current density profile between the two cathode configurations. The in-plane configuration enhances the thruster performance compared with the out-of-plane configuration by increasing the percentage of beam ions. This section will discuss the possible causes of the observed changes in ion current density, as well as possible impacts on HET testing.

A hollow cathode is not solely an electron source. The emitted electrons are also accompanied by cathode ions and unionized neutrals. Each of these three species (ions, neutrals, and electrons) may affect the plume ion current density profile of the HET as seen in the plume measurements. The largest change in plume properties due to cathode location is the significant increase in the left ion current density peak with the in-plane configuration. The measured ion beam current is also larger for the in-plane configuration, whereas the discharge current is nearly constant. As the in-plane cathode is located on the left side of the thruster, this suggests that the cathode increases the local ion current density and the total ion current. To identify the contribution of each cathode exhaust species on the local ion current density, we perform an order of magnitude analysis.

A. Cathode Ions

Emitted cathode ions are typically low energy, on the order of 1 eV [21]. Likewise the potential drop experienced by cathode ions is less than 5 V. The external electric fields outside the channel are also very small, 1–2 V/cm [24–26]. In the T-220HT, the local magnetic fields near the cathode are parallel with the cathode, providing little resistance to electron motion, thus little to no electric field is developed. If the ions contribute a significant amount to the total beam current, the effect would appear as a sharp increase in ion energy at low levels (less than 10 V). Instead, as can be seen in Figs. 9 and 10, the in-plane cathode configuration has a consistent increase in the raw collected current across the entire voltage range. This suggests that the ions that increase the ion current density in the region of the cathode also experience the same acceleration profile as ions that originate from the HET discharge channel.

Consider the number of ions produced by the cathode. The majority of cathode ions produced within the orifice region are lost to self-heating collisions with the cathode surfaces. The emitted ion number density is typically much less than the electron density. Kameyama and Wilbur [23] experimentally measured the ion density 180 mm downstream of a hollow cathode. They obtained densities on the order of 1×10^{11} m^{-3} for xenon propellant at 3–5 standard cubic centimeters per minute (sccm, 0.3–0.49 mg/s) flow rate. That is approximately half of the equivalent cathode flow rate in krypton used in this work, thus the same magnitude of ion density can be expected. Compared with the typical discharge ion density of 10^{17}–10^{18} m^{-3} seen in HETs [24,27], the cathode ions are a negligible factor. For this investigation, the contribution from cathode ions does not account for the measured increase in ion current density in the in-plane cathode configuration.

B. Cathode Neutrals

The second species to consider is cathode neutrals. From the out-of-plane plume data, it appears the thruster has a lower density of ions at −90 deg, which may be due to nonuniform propellant distribution by the anode or possible nonuniformities in the vacuum. The anode nonuniformity was confirmed post testing with flame visualization [28]. Figure 12 shows the results of the flame visualization with premixed air and propane. The flame was first ignited at fuel rich conditions and makes evident a leak in the anode side wall. At stoichiometric fuel conditions, the leak does not ignite, but still causes visible flow nonuniformity in the nearby anode orifices. The leak reduces the axial propellant flow in that region, thereby decreasing the neutral density.

The in-plane cathode may provide an influx of neutrals that is ingested by the thruster and ionized to cause the observed increase in the left ion current peak. To determine if neutrals are a possible factor, we can compare the neutral density and ingestion from the cathode

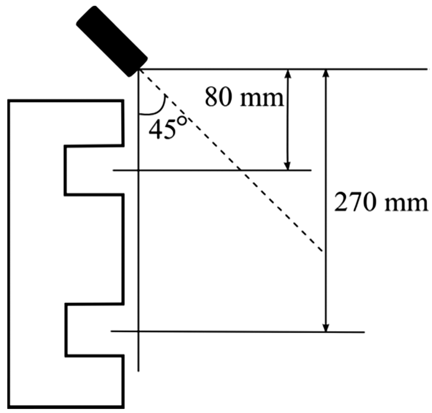

Fig. 13 A 45 deg expansion of cathode neutrals into the vacuum relative to thruster geometry.

across the channel. The neutral density at the cathode orifice can be calculated from the ideal gas law. The orifice pressure can be found from Poiseuille's law for viscous gases in a cylindrical container. The result from Goebel and Katz is [29]

$$P = \sqrt{\frac{0.78Q\zeta l(T/289.7)}{d^4}} \tag{2}$$

where P is the orifice neutral gas pressure in torr, Q is the mass flow rate in sccm, ζ is the gas viscosity in poise ($1\ \mathrm{P} = 0.1\ \mathrm{Pa \cdot s}$), T is the gas temperature in Kelvin, and l and d are the length and diameter of the cathode orifice opening in centimeters, respectively. The cathode flow rate was kept constant at 16 sccm (1 mg/s) throughout the tests. The thermionic emission temperature for cathode inserts is $\sim$1000°C, though actual temperatures are typically two to three times that [4,29]. An average temperature of 2000 K will be assumed here based on values calculated by Mikellides et al. for hollow cathodes [30]. The viscosity for krypton at that temperature is $107.5 \times 10^{-6}\ \mathrm{Pa \cdot s}$ [30]. The EPL 375 cathode orifice is 0.16 cm long and 0.15 cm in diameter. The neutral pressure at the orifice is thus 5.3 torr, which gives a neutral density of $2.54 \times 10^{22}\ \mathrm{m^{-3}}$ from the ideal gas law. We will assume that the neutral gas expands at a 45 deg half-angle downstream of the orifice as shown in Fig. 13 for simplicity [29]. The resultant expansion cone crosses the thruster channel centerline at 80 and 270 mm from the cathode. The cross-sectional areas at those two locations are 3080 and 32280 times greater than the orifice area. The channel area nearest the cathode thus sees a neutral density of $8.26 \times 10^{18}\ \mathrm{m^{-3}}$, whereas the far side sees a density of $7.88 \times 10^{17}\ \mathrm{m^{-3}}$. This is an order of magnitude difference in neutral densities. These values are also greater than the chamber neutral density, which is approximately $3 \times 10^{17}\ \mathrm{m^{-3}}$.

The ingestion rate of neutrals can be calculated from Eq. (3) for a free molecular flux [31,29]:

$$\dot{N} = \frac{n\bar{c}}{4}A \tag{3}$$

$$\bar{c} = \sqrt{\frac{8kT}{\pi m}} \tag{4}$$

where $\dot{N}$ is the neutral ingestion rate in particles per second, n is the neutral number density, $\bar{c}$ is the neutral thermal velocity calculated by Eq. (4), A is the ingestion area of the channel, k is Boltzmann's constant, and m is the mass of krypton. The neutrals are assumed to still be 2000 K, and the ingestion area is taken to be 10% of the total channel area to reflect the fact the neutral density changes across the channel. With the previous neutral density values for the near and far sides of the channel, the resulting ingestion rate is 2.76×10^{18} and $2.64 \times 10^{17}\ \mathrm{s^{-1}}$, respectively. This is equivalent to 0.387 and 0.0369 mg/s of krypton mass flow rate. Again, this is an order of magnitude difference in neutral ingestion. The difference of 0.35 mg/s is equivalent to roughly 0.25 A of beam current, assuming an average conversion of $0.7\ \mathrm{A \cdot mg^{-1} \cdot s^{-1}}$ for krypton based on the measured ion beam current. This matches relatively well to the observed increase in beam current due to the in-plane cathode ($\Delta I_b = 0.43$, 0.34, 0.02, and 0.03 A for 300–150 V). Thus, the increase in the left ion current density peak can be at least partly attributed to the local ingestion of cathode neutrals. The lack of change to the right current density peak is similarly due to only 0.0369 mg/s of cathode neutrals at the far side based on this simple analysis. This analysis makes simplifying assumptions to gain a basic understanding of the effect of the neutrals. In reality, the cathode neutrals likely diffuse at a larger angle than 45 deg. This will further enhance neutral ingestion for the near channel and reduce ingestion for the far channel. The thruster ingestion of said neutrals also occurs in a continuous fashion across the whole face of the channel, likely further reducing cathode neutrals at the far side of the channel. The ingestion of cathode neutrals likely occurs for any cathode, irrelevant of placement; it is mainly an issue of nonuniform ingestion. If the chamber pressure were high enough to give background density equal to the cathode expansion ($\sim 3 \times 10^{-4}$ torr), the effects of cathode neutral ingestion by the thruster would not be seen because they would be overridden by the ingestion of chamber neutrals.

With increased neutral density near the cathode, the effect of charge-exchange collisions should be considered. Charge-exchange collisions typically increase slow ion flux, thereby increasing the measured ion current density at large angles. However, as the in-plane data shows, the presence of the cathode at the left side of the plane actually decreases the measured ion flux. Thus, if charge-exchange collisions do increase, it is a minor effect. The decrease in ion flux at negative angles may be due to cathode electrons, which is discussed in the next section.

The ion energy distribution between the two cathode configurations showed little to no change. This fact suggests that the ion beam current is increased by the ingestion of neutrals, as opposed to the ion being further accelerated or decelerated. This is an expected behavior, as neutral ingestion does not change the ionization and acceleration processes in HETs. This increase in the ion beam with the in-plane cathode can be seen in the raw RPA measurements shown in Figs. 9 and 10. The in-plane raw ion current measurement is higher than the out-of-plane measurement.

C. Cathode Electrons

The final contribution from the cathode is electrons. The external placement of the cathode means that electrons are injected into the thruster and thus the Hall current at one azimuthal location. There are three major electron motions that occur: the electron's motion along the local magnetic field lines into the channel, an $E \times B$ drift motion to distribute them around the annulus, and finally a cross-field motion toward the anode. It is possible that the azimuthally localized injection of electrons into the Hall current creates differences in electron density with commensurate differences in the ionization rate at different azimuthal locations in the channel. We can examine this effect by considering the relative time and velocity scales of the three motions.

The electron injection time scale is calculated with the straight line distance from the cathode to the near and far sides of the discharge channel, divided by the electron thermal velocity. Cathode electrons, like ions, have relatively low energies of a few electron volts. With a temperature of 2 eV, the electron thermal velocity is 9.5×10^5 m/s. Using the 80 mm distance from the neutral density analysis, the time scale of electron injection is 8×10^{-8} s.

The $E \times B$ time scale is taken as the average time an electron takes to complete one circuit of the annulus. The $E \times B$ drift velocity is given by

$$c_{E\times B} = \frac{\mathbf{E} \times \mathbf{B}}{|\mathbf{B}|^2} = \frac{E}{B} \tag{5}$$

where $\mathbf{E}$ and $\mathbf{B}$ are the electric and magnetic field vectors, and E and B are their respective magnitudes. The peak magnetic field strength in

Table 2 Values used to calculate the cross-field electron mobility

Parameter	Value
n_n	1×10^{19} m^{-3}
n_e	1×10^{11} m^{-3}
T_e	2 eV
σ_{en} at 2 eV	3.11×10^{-20} m^2
$c_e = \sqrt{8kT_e/\pi m_e}$	9.46×10^6 m/s
$\ln \Lambda$	10
B	0.02 T
ν_{ei}	1.03 s^{-1}
ν_{en}	2.94×10^5 s^{-1}
ν_B	5.63×10^{10} s^{-1}

the channel, where the Hall current exists, is 200 G. The electric field at that point varies depending on discharge condition and was not measured here. An average value of 100 V/cm will be assumed based on published research of similar HETs [24,26,32]. The resulting drift velocity is 5×10^5 m/s. With a mean channel circumference of 0.59 m, the time scale for the $E \times B$ drift is approximately 1×10^{-6} s.

Finally, the cross-field drift of electrons can be described by the cross-field electron mobility $\mu_{e\perp}$ [29]:

$$\mu_{e\perp} = \frac{e}{m_e \nu_m} \frac{1}{1 + \omega_c^2/\nu_m^2}$$

where $\omega_c = eB/m_e$ is the electron gyro frequency and ν_m is the momentum collision frequency. The cross-field motion is affected by electron–ion collisions, electron–neutral collisions, and Bohm diffusion. The electron–neutral and electron–ion collision frequencies are given by $\nu_{\mathrm{en}} = n_n \sigma_{\mathrm{en}} c_e$ and $\nu_{\mathrm{ei}} = 2.9 \times 10^{-12} n_e \ln \Lambda T_e^{-3/2}$. An effective Bohm frequency can be taken as $\nu_B = 16\omega_c$, where the constant is the Bohm diffusion coefficient [29]. The total momentum collision cross section is the sum of these three components. From the values given in Table 2, it is clear that the cross-field mobility is dominated by Bohm diffusion. The resultant cross-field mobility is thus 0.194 m^2/V · s. Using the previous assumed electric field of 100 V/cm, the cross-field velocity is thus 1940 m/s.

The three motions have very disparate velocities and time scales. Electron injection from the cathode is the fastest, at least two orders of magnitude faster than the others. This suggests that electrons are injected into the thruster much faster than the drift velocity can evenly distribute them. However, the rate limiting step that controls ionization is the cross-field diffusion. An azimuthal variation in electron density is possible, but only at the most downstream location where electrons are injected. The slow cross-field diffusion means that electrons are essentially uniformly distributed around the channel in the time it takes to cross a field line towards the anode. There is thus unlikely to be a large amount of localized ionization except near the injection point.

The electron calculations may also explain some of the HET ignition data. The high-speed pictures by Ellison et al. [7] show a phenomenon during HET ignition wherein the discharge level varies azimuthally but is strongest near the cathode. This provides evidence that a difference between electron injection and distribution time scales exists. As Ellison's images show, after ~50 μs the nonuniformity disappears, which can be explained by the rate limiting cross-field diffusion causing uniform ionization. The fact the external cathode is at a noncentral location also explains the decrease in ion current seen at large angles. The noncentralized position of the cathode also affects the electrons dispersed into the plume for neutralization. A higher density of electrons will exist in the plume region near the cathode compared with the plume 180 deg from the cathode. This can reduce the number of ions in the plume near the cathode. The electrons likely contribute to the decreased ion current density at large negative angles in the ion current profile.

V. Conclusions

The T-220HT HET was tested with the cathode located in and out of the plane of probe measurements. There is a noticeable change in the plume current density profile from the out-of-plane cathode configuration to the in-plane cathode configuration. The in-plane cathode increased the ion current density for one side of the plume. The ion energy was unaffected by the location of the cathode. A simple analysis of cathode species shows that the observed changes are caused by a regional increase in cathode electrons and neutrals due to the external placement of the cathode. These results show that an external cathode causes significant azimuthal asymmetry in the far-field plume of a HET. The external cathode contributes neutrals and electrons nonuniformly to the plume and thruster. This has the effect of increasing ion flux in regions in proximity to the cathode. Ion current flux measurement of the entire plume would be necessary to better characterize the full three-dimensional effect of the external cathode.

The results suggest that care should be taken in testing and integrating HETs with external cathodes. It should be noted that the species contributed by the cathode to the thruster and plume are always present. With internal cathodes, the species are evenly distributed into the channel and plume. With external cathodes, there is a spatial variation due to the expansion of the cathode species from a noncentralized location. Thus, for external cathodes, it may be impossible to avoid cathode contributions. The question then becomes how to minimize the external cathode effects for plume measurements or for satellite integration.

To avoid external cathode nonuniformity in plume measurements, the cathode should be located perpendicular to the plane of measurements to allow for symmetric cathode effects across the plane of measurement. If an in-plane cathode is unavoidable, the peak current density should be decreased by 10–40% depending on flow rates and voltages to adjust for the cathode species. For a uniform anode propellant distribution, this effect may be seen as uneven peaks in the ion current density profile. The divergence angle changes are small compared with the uncertainty, and thus no adjustment is necessary. For satellite integration, the orientation of an externally mounted cathode should be considered for the potential of ion bombardment due to the expanded plume. A likely solution is to orient the cathode 180 deg from the nearest satellite structure.

Appendix: Data for the Thruster Conditions Tested in this Work

Table A1 Data for the thruster conditions tested in this work

Cathode location	Discharge voltage V_d, V	Discharge current I_d, A	Total mass flow, mg/s	Beam current I_b, A	Plume half-angle, deg	V_{mp} centerline, V	V_{mp} 60 deg, V	V_{cg}, V
Out of plane	300	8.98	8.08	6.33	62.19	259.8	257.9	−23.6
	250	9.05	9.1	6.64	64.25	— —	— —	−22.3
	200	8.95	9.26	6.19	69.32	— —	— —	−20.6
	150	8.95	9.86	5.65	73.65	107.1	110.2	−18.2
In plane	300	9.03	8.29	6.76	60.87	257.7	260.0	−21.9
	250	9.02	8.5	6.98	62.61	— —	— —	−22.0
	200	9.01	8.64	6.21	66.69	— —	— —	−21.1
	150	9.02	8.85	5.68	73.05	106.9	115.2	−19.0

Acknowledgments

The research contained herein is sponsored by Moog In-Space Propulsion (formerly American Pacific In-Space Propulsion). We would like to thank Pratt and Whitney Rocketdyne for supplying High-Power Electric Propulsion Laboratory (HPEPL) with the T-220HT, Gregory McCormick for work in simulation and modifications, Hoang Dao for programming assistance, and departmental technical staff and other graduate students at HPEPL for assistance with this work.

References

[1] Smirnov, A., and Raitses, Y., "Plasma Measurements in a 100 W Cylindrical Hall Thruster," *Journal of Applied Physics*, Vol. 95, No. 5, 2004, pp. 2283–2292.
doi:10.1063/1.1642734

[2] Jameson, K. K., Goebel, D. M., Hofer, R. R., and Watkins, R. M., "Cathode Coupling in Hall Thrusters," IEPC Paper 2007-278, 2007.

[3] McDonald, M. S., and Gallimore, A. D., "Cathode Position and Orientation Effects on Cathode Coupling in a 6-kW Hall Thruster," IEPC Paper 2009-113, 2009.

[4] Sommerville, J., "Hall-Effect Thruster–Cathode Coupling," Ph.D. Dissertation, Dept. of Mechanical Engineering, Michigan Technological Univ., Houghton, MI, 2009.

[5] Parra, F., and Ahedo, E., "A Two-Dimensional Hybrid Model of the Hall Thruster Discharge," *Journal of Applied Physics*, Vol. 100, No. 2, 2006, Paper 023304.
doi:10.1063/1.2219165

[6] Bourgeois, G., Mazouffre, S., and Sadeghi, N., "Unexpected Transverse Velocity Component of Xe[sup +] Ions Near the Exit Plane of a Hall Thruster," *Physics of Plasmas*, Vol. 17, No. 11, 2010, Paper 113502.
doi:10.1063/1.3507308

[7] Ellison, C. L., Raitses, Y., and Fisch, N. J., "Fast Camera Imaging of Hall Thruster Ignition," *IEEE Transactions on Plasma Science*, Vol. 39, No. 11, 2011, pp. 2950–2951.
doi:10.1109/TPS.2011.2121925

[8] McVey, J. B., Britt, E. J., Engelman, S. F., Gulczinski, F. S., Beiting, E. J., and Pollard, J. E., "Characteristics of the T-220HT Hall-Effect Thruster," AIAA Paper 2003-5158, 2003.

[9] Electric Propulsion Lab., "EPL HCPEE 375 Manual," 2012.

[10] Manzella, D. H., and Sankovic, J. M., "Hall Thrusters Ion Beam Characterization," AIAA Paper 1995-2927, 1995.

[11] Walker, M. L. R., Hofer, R. R., and Gallimore, A. D., "The Effects of Nude Faraday Probe Design and Vacuum Facility Backpressure on the Measured Ion Current Density Profile of Hall Thruster Plumes," AIAA Paper 2002-4253, 2002.

[12] Hofer, R. R., Walker, M. L. R., and Gallimore, A. D., "A Comparison of Nude and Collimated Faraday Probes for Use with Hall Thrusters," IEPC Paper 2001-020, 2001.

[13] Mason, L. S., and Jankovsky, R. S., "1000 Hours of Testing on a 10 Kilowatt Hall Effect Thruster," AIAA Paper 2001-3773, 2001.

[14] Brown, D. L., and Gallimore, A. D., "Evaluation of Facility Effects on Ion Migration in a Hall Thruster Plume," *Journal of Propulsion and Power*, Vol. 27, No. 3, 2011, pp. 573–585.
doi:10.2514/1.B34068

[15] Brown, D. L., and Gallimore, A., "Evaluation of Ion Collection Area in Faraday Probes," *Review of Scientific Instruments*, Vol. 81, No. 6, 2010, Paper 063504.
doi:10.1063/1.3449541

[16] King, L. B., "Transport-Property and Mass Spectral Measurements in the Plasma Exhaust Plume of a Hall-Effect Space Propulsion System," Ph.D. Dissertation, Dept. of Aerospace Engineering, Univ. of Michigan, Ann Arbor, MI, 1998.

[17] Hutchinson, I. H., *Principles of Plasma Diagnostics*, Cambridge Univ. Press, Cambridge, England, U.K., 1987.

[18] Xu, K. G., "Ion Collimation and In-Channel Potential Shaping Using In-Channel Electrodes for Hall Effect Thrusters," Ph.D. Dissertation, Dept. of Aerospace Engineering, Georgia Inst. of Technology, Atlanta, GA, 2012.

[19] Brown, D. L., "Investigation of Low Discharge Voltage Hall Thruster Characteristics and Evaluation of Loss Mechanisms," Ph.D. Dissertation, Dept. of Aerospace Engineering, Univ. of Michigan, Ann Arbor, MI, 2009.

[20] Linnell, J. A., "An Evaluation of Krypton Propellant in Hall Thrusters," Ph.D. Dissertation, Dept. of Aerospace Engineering, Univ. of Michigan, Ann Arbor, MI, 2007.

[21] Dushman, S., *Scientific Foundations of Vacuum Technique*, Wiley, New York, 1958, 80–81.

[22] Friedly, V. J., and Wilbur, P. J., "High Current Hollow Cathode Phenomena," *Journal of Propulsion and Power*, Vol. 8, No. 3, 1992, pp. 635–643.
doi:10.2514/3.23526

[23] Kameyama, I., and Wilbur, P. J., "Characteristics of Ions Emitted from High-Current Hollow Cathodes," IEPC Paper 1993-023, 1993.

[24] Reid, B. M., "The Influence of Neutral Flow Rate in the Operation of Hall Thrusters," Ph.D. Dissertation, Dept. of Aerospace Engineering, Univ. of Michigan, Ann Arbor, MI, 2009.

[25] Xu, K. G., Dao, H., and Walker, M. L. R., "Potential Contour Shaping and Sheath Behavior with Wall Electrodes and Near-Wall Magnetic Fields in Hall Thrusters," *Physics of Plasmas*, Vol. 19, No. 20, 2012, Paper 103502.
doi:10.1063/1.4762856

[26] Linnell, J. A., and Gallimore, A. D., "Internal Plasma Structure Measurements of a Hall Thruster Using Plasma Lens Focusing," AIAA Paper 2005-4402, 2005.

[27] Shastry, R., Gallimore, A., and Hofer, R. R., "Near-Wall Plasma Properties and EEDF Measurements of a 6-kW Hall Thruster," AIAA Paper 2009-5356, 2009.

[28] Langendorf, S., and Walker, M. L. R., "Characterization of Hall Effect Thruster Propellant Distributors with Flame Visualization," *Review of Scientific Instruments*, Vol. 84, No. 1, 2013, Paper 013302.
doi:10.1063/1.4774049

[29] Goebel, D. M., and Katz, I., *Fundamentals of Electric Propulsion: Ion and Hall Thrusters*, Jet Propulsion Lab., Pasadena, CA, 2008, pp. 465, 258, 289, 33, 368.

[30] Mikellides, I. G., Katz, I., Goebel, D. M., and Polk, J. E., "Hollow Cathode Theory and Experiment 2: A Two-Dimensional Theoretical Model of the Emitter Region," *Journal of Applied Physics*, Vol. 98, No. 11, 2005, Paper 113303.
doi:10.1063/1.2135409

[31] Ketsdever, A. D., Lee, R. H., and Lilly, T. C., "Performance Testing of a Microfabricated Propulsion System for Nanosatellite Applications," *Journal of Micromechanics and Microengineering*, Vol. 15, No. 12, 2005, pp. 2254–2263.
doi:10.1088/0960-1317/15/12/007

[32] Haas, J. M., "Low-Perturbation Interrogation of the Internal and Near-Field Plasma Structure of a Hall Thruster Using a High-Speed Probe Positioning System," Ph.D. Dissertation, Dept. of Aerospace Engineering, Univ. of Michigan, Ann Arbor, MI, 2001.

J. Blandino
Associate Editor